frontiers | Frontiers in Materials

TYPE Original Research
PUBLISHED 13 October 2022
DOI 10.3389/fmats.2022.1013545

OPEN ACCESS

EDITED BY
Neven Ukrainczyk,
Darmstadt University of Technology, Germany

REVIEWED BY
Zeynep Basaran Bundur,
Özyeğin University, Turkey
Zhiyong Liu,
Southeast University, China

*CORRESPONDENCE
Xiaowei Cheng,
chengxw@swpu.edu.cn

SPECIALTY SECTION
This article was submitted to Energy Materials,
a section of the journal
Frontiers in Materials

RECEIVED 07 August 2022
ACCEPTED 03 October 2022
PUBLISHED 13 October 2022

CITATION
Xing X, Zhong G, Wu Z, Cai J and Cheng X (2022), Self-healing mechanism of deposited carbonates in cement cracks under CO_2 storage well conditions.
Front. Mater. 9:1013545.
doi: 10.3389/fmats.2022.1013545

Self-healing mechanism of deposited carbonates in cement cracks under CO_2 storage well conditions

Xuesong Xing[1], Guangrong Zhong[2], Zhiqiang Wu[1], Jingxuan Cai[3,4] and Xiaowei Cheng[3,4]*

[1]CNOOC Research Institute Co.,Ltd., Beijing, China, [2]CNPC Chuanqing Drilling Engineering Co.,Ltd., Chuandong Drilling Company, Chongqing, China, [3]School of New Energy and Materials, Southwest Petroleum University, Chengdu, China, [4]Key Laboratory of Oil and Gas Reservoir Geology and Exploitation, Southwest Petroleum University, Chengdu, China

In CO_2 geological storage wells, the leakage of CO_2 along the micro-cracks of the cement sheath of abandoned wells is one of the main risks of CO_2 leakage. The chemical reaction between CO_2 and oil well cement can realize self-healing of micro-cracks in the cement sheath. In this study, self-healing experiments of artificial cracks in cement-based materials were carried out by simulating the working conditions of high temperature, high pressure and CO_2-rich CCS. The formation process and self-healing effect of calcium carbonate ($CaCO_3$) in oil well cement-based materials induced by CO_2 under different exposure environments were explored, and the self-healing products were analyzed by X-ray diffraction (XRD) and environmental scanning electron microscopy (ESEM and EDX). X-ray computed tomography (μ-CT) was used to reconstruct the changes of cracks in 3D, and compressive strength, porosity, and permeability were used to evaluate the self-healing properties of cement-based material cracks. The results indicated that for the CS-28 (the samples reacted with humid CO_2 for 28 days) and AS-28 (the samples reacted with humid air for 28 days) samples, the compressive strength increased by 56.67% and 10.38%, the porosity decreased by 59.37% and 18.19%, and the permeability decreased by 59.91% and 28.07%, respectively. The crack-volume reduction rate of the CS-28 specimen was 57.08%, and the pore-volume reduction rate was 69.20%. Many massive, needle shaped $CaCO_3$ crystals were formed in the pores and cracks of the sample. The reconstruction of the 3D structure of self-healing cement shows that the micro-cracks of the cement are sealed but the pores are increased. The damage prediction based on von Mises stress shows that under the axial force, the healing layer is not prone to damage. This study provides a theoretical and experimental basis for applying self-healing technology in CCS downhole environment, improving the service life of cement sheath and preventing the leakage of stored CO_2.

KEYWORDS

carbon capture and storage, cracks, self-healing, $CaCO_3$, oil-well cement

Introduction

Climate change caused by greenhouse-gas emissions is one of the main crises currently facing global society (Gerres et al., 2019). CO_2 in the atmosphere is one of the main causes of global warming, accounting for >72% of total greenhouse-gas emissions (Abid et al., 2020). The key factors that determine the concentration of CO_2 in the atmosphere are economic, social, and technological changes and human and natural development (Nakicenovic et al., 2000). Various energy-intensive industries are the main sources of carbon emissions. Therefore, it is essential to develop a series of technologies to reduce CO_2 emissions and capture them from the atmosphere in response to climate change.

Carbon capture and storage (CCS) is a way to reduce the amount of CO_2 emitted into the atmosphere as a result of human activities (Costa et al., 2019). CCS is currently considered to be one of the most effective technologies for reducing CO_2 emissions (Leung et al., 2014; Dindi et al., 2019; Garcia et al., 2019; Thengane et al., 2019). Typically, abandoned oil and gas well are the main subjects for CO_2 storage (Bachu and Watson, 2009). The success of a CCS project depends on the integrity of the reservoir and the completion materials used to close the injection interval (Shah and Bishnoi, 2018). The main challenges include preventing carbon dioxide from escaping to the atmosphere after storage and achieving safe storage.

Researchers have conducted many experiments to investigate different approaches of CO_2 leakage. These studies revealed that the main leakage pathways are the gap between the surrounding rock and the cement well sheath (Zhang et al., 2019), the gap between the casing and the cement sheath, and the cracks in the cement sheath. Chemical damage and mechanical failure of the cement sheath are the most important threats to the long-term integrity of CO_2 storage wells. In general, under reservoir conditions, microcracks appear on the cement sheath owing to the dual effects of external loads and internal stresses, providing a pathway for CO_2 leakage and resulting in more severe leakage accidents, which directly threatens human and environmental safety (Costa et al., 2017). Several different solutions have been proposed for this problem. For example, a system in which additives such as fibers or elastomers are added to the cement slurry to improve the performance of the cement sheath and promote the self-healing of the cracked cement sheath was proposed.

The self-healing phenomenon was first reported by the French Academy of Sciences in 1836 (Palin et al., 2015). To improve the ability of cementitious materials to prevent cracks, inhibit the invasion of harmful substances, and extend the service life, self-healing technology for concrete has been thoroughly studied. Many methods for obtaining self-healing concrete have been reported, employing microcapsules, microbes, cementitious materials, and shape-memory alloys. Researchers divide self-healing cement-based materials into two categories—autogenous healing and autonomous healing—according to the self-healing mechanism (Tang et al., 2015; Li et al., 2019). Autogenous healing is attributed to the unreacted cement particles and carbonization of hydration products, which forms calcium carbonate ($CaCO_3$) deposits in cement-based materials. CO_2 induced cement self-healing is based on the deposition of calcium carbonate on the surface of cement cracks. Many researchers have reported on self-healing of cement composites in CO_2 environment. These studies reported the addition of crystallization-inducing additives to cement-based materials to promote the formation of calcium carbonate. Sahmaran et al. (2013) investigated the effects of different supplementary cementitious materials (SCM) on self-healing properties. Wang conducted an experimental study on the self-healing potential of concrete. This study investigated the effects of crystalline admixture on self-healing properties crystalline admixture (Wang et al., 2018a). Pejman et al. (2019) investigated the calcium carbonate precipitation induced by bacteria, which has the potential to improve self-healing ability. However, the study on the self-healing of oil well cement under the condition of CO_2 storage in abandoned oil and gas wells is rare. Autonomous healing relies primarily on healing agents that are not part of the cement-based materials. Research on self-healing of concrete has mainly focused on autonomous healing using bacteria (Wang et al., 2014a; Wang et al., 2014b; Luo et al., 2015; Gupta et al., 2018; Su et al., 2019), microcapsules (Rupnow et al., 2017; Wang et al., 2018b; Zha et al., 2018), or organic or inorganic materials (Gupta et al., 2018; Li et al., 2019; Su et al., 2019). Additionally, superabsorbent polymers have been used as self-healing agents to seal concrete cracks (Klemm and Sikora, 2013; Jiang et al., 2015; Suleiman et al., 2019). However, many problems limit the application of cement-based materials, such as their high prices and poor mechanical properties. Autogenous healing methods have been investigated for many years. However, studies have indicated that the crack-filling fraction for this method in 200 h is approximately 42% (Liu et al., 2017), which cannot satisfy the needs of the self-healing system. Therefore, researchers began to optimize and increase the healing speed of cracks in cement-based materials according to the autogenous healing mechanism. There are two main types of optimization methods. One involves accelerating the hydration process (Wang et al., 2020a), and the other involves inducing the deposition of calcium carbonate (Wang et al., 2020b).

Additionally, researchers have evaluated the effects of the self-healing humidity, temperature, and age, as well as other environmental factors (Huang et al., 2013; Jiang et al., 2015; Palin et al., 2015; Gwon et al., 2019; Suleiman et al., 2019), on the self-healing performance of cement-based materials. Palin et al. (2015) studied the autogenous healing ability of ordinary Portland cement (OPC) and blast furnace slag (BFS) cement mortar samples submerged in fresh water and seawater. After 56 days, the BFS cement in the seawater cured 100% of the cracks to 104 μm, while the value for the OPC specimen was 592 μm. In

TABLE 1 Compositions of cement slurry.

Materials	Class G oil well cement	Micro silicon	G33S	SXY-2
Percentage (wt/%)	100	10	1.5	1

the fresh water, 100% of the cracks in the BFS specimen were cured to 408 μm, and 100% of the cracks in the OPC specimen were cured to 168 μm. A. R. Suleiman et al. (Ferrara et al., 2017) studied the self-repairing of cracks in cement mortar under different exposure conditions. A sample of pre-cracked mortar was immersed in water, and the same sample was exposed to cycling of the temperature and relative humidity. The results indicated that the self-healing of cracks is more favorable in the presence of water. Additionally, the effectiveness of cement-based materials for self-healing of cracks depends largely on the surrounding environment.

This article combines previous research on the carbonization of cement-based materials (Duguid and Scherer, 2010; Jung and Um, 2013; Yuanhua et al., 2013; Roig-Flores et al., 2015; Shah and Bishnoi, 2018; Suleiman and Nehdi, 2018) and the effects of self-healing mechanisms and environmental factors. A self-healing experiment was performed by simulating the downhole environment of CCS. The crack self-healing ability (crack filling rate and filling material) of cement-based materials in CO_2-rich environment was evaluated. The self-healing performance of cement-based material cracks was evaluated by testing compressive strength, porosity and permeability. The self-healing products were analyzed and observed by X-ray diffraction (XRD) and environmental scanning electron microscopy (ESEM and EDX). Three-dimensional reconstruction of crack changes was carried out by X-ray computed tomography (CT), and crack healing was discussed. The von Mises stress distribution of the cement matrix after healing was simulated by the finite element method, and the damage prediction was carried out. The research results provide a certain experimental and theoretical basis for the application of cement self-healing technology in CCS wells to improve the integrity of the cement sheath and reduce the leakage of CO_2 stored in CCS wells.

Materials and experiments

Materials

G-class oil-well cement of Sichuan Jiahua Co., Ltd. and Silica Fume of Omax Co., Ltd. were used in the experiment. The filtrate reducer and disperser were G33S and SXY-2, respectively, and were produced by Weihui Co., Ltd.

Sample preparation

The water-solid ratio (w/s) of the G-class oil-well cement slurries was 0.44. Cement slurries were weighed and mixed according to the Table 1 presented below. The percentages in the tabular refer to mass ratios.

According to API RP 10B-2 (API-RP-10B-2, 2013), weigh the weight of cement, admixtures and mixing water, and thoroughly mix the dry cement powder and admixtures evenly. Then, add it to the slurry cup and stir evenly at a low speed (4,000 ± 200 r/min). The mixed powder should be added to the slurry cup within 15 s, and then stirred at high speed (12,000 ± 500 r/min) for 35 s ± 1 s. Cement samples were then cast into molds of different specifications and cured for 28 days at 90°C and 100% relative humidity. The molds used to test compressive strength and porosity are 50 mm × 50 mm×50 mm and φ25 mm × 25 mm respectively. After the slurry was cured for 28 days, the experimental samples were removed and cracked. The cracked samples were numbered separately and placed in a cement self-healing reactor, as shown in Figure 1. The width of the crack on the outer edges is 0.8 mm. The width of the crack in the middle of the sample is 0.3 mm.

CO_2 is injected generally in a supercritical form into underground formations (Energy Institute, 2010). To simulate the CCS downhole environment and ensure that the CO_2 was in a supercritical state, the CO_2 pressure was set as 5.0 MPa, with a total pressure of 8.0 MPa. The experimental temperature of the sample was set as 90°C. The samples reacted with gaseous supercritical CO_2 containing water vapor for 0, 3, 7, and 28 days. The CO_2 gas consumed during the experiment was replenished. The naming rules of the samples are presented in Table 2.

Characterization

The self-healing ability in two environments was evaluated by testing the compressive strength, porosity, and gas-permeability recovery of the samples before and after self-healing. All the samples were dried for at least 24 h at 60 ± 3°C. The average of three measurements was recorded for each sample. The porosity was calculated as follows:

$$\Phi = \left(1 - \frac{V_s}{V_f}\right) \times 100\%,$$

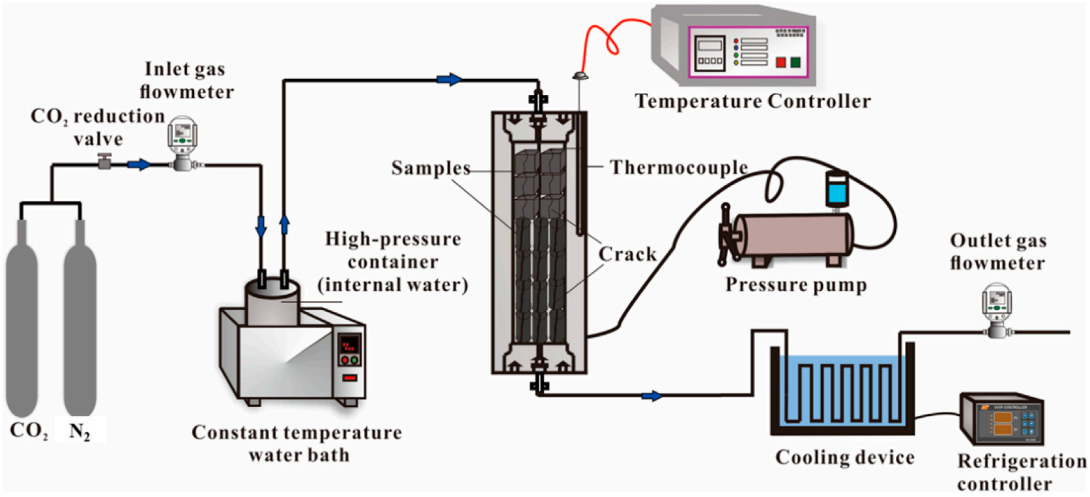

FIGURE 1
Schematic of the cement self-healing equipment.

TABLE 2 Naming rules of the Self-healing test specimens.

Group	Medium	Broken age period (days)	specimens
AS	Moist air	0, 3, 7, 28	AS-0, AS-3, AS-7, AS-28
CS	Moist CO_2	0, 3, 7, 28	CS-0, CS-3, CS-7, CS-28

where Φ represents the core porosity (in %), V_s represents the skeleton volume of the core (in cm^3), and V_f represents the apparent volume of the core (in cm^3).

The permeability calculation formula is as follows:

$$K = \frac{2PQL\mu}{A\left(P_1^2 - P_2^2\right)} \times 10^2,$$

Where K represents the permeability (in md), P represents the atmospheric pressure (in MPa), Q represents the gas volume flow at the outlet of the rock sample (in cm^3/s), L represents the length of the rock sample (in cm), μ represents the viscosity of the gas (in mPa·s), A represents the cross-sectional area of the rock sample (in cm^2), P_1 represents the absolute pressure at the inlet of the rock sample (in MPa), and P_2 represents the absolute pressure at the outlet of the rock sample (in MPa).

X-ray micro-computed tomography (μ-CT) was used analyze the crack changes. Reconstruction of the projections was performed using the software VGStudio MAX 3.0 (Volume Graphics Co., Germany). Based on the reconstructed three-dimensional structure and the finite element analysis method, the von Mises stress distribution simulation of the self-healing cement matrix is performed through the software VGStudio MAX 3.0 (Volume Graphics Co., Germany).

Analysis and observation of the micromorphology of the crack surface and the self-healing products were performed *via* environmental scanning electron microscopy (ESEM) (Quanta 450, FEI Co. Ltd., United States). Simultaneously, energy-dispersive X-ray spectroscopy (EDX) and X-ray diffraction (XRD) for elemental analysis of the self-healing products in the crack gap were performed to verify the self-healing mechanism. The detailed parameters of each characterization method are presented in Table 3.

Results and discussion

XRD analysis

The XRD results for the control and self-healing samples at different cracking ages are presented in Figure 2. Figure 2A shows the XRD patterns of the AS samples. Prominent peaks of CH (PDF # 44-1481) were observed at 2θ = 18.0°, 34.1°, 47.1°, and 50.8°, and as the self-healing process continued, the CH peak strength increased. The results indicate that during the self-healing process of the AS samples, the main product was the hydration product (CH) of the cement-based materials. Therefore, the hydration of unhydrated cement particles was the main reaction of the AS sample during the self-healing process, and it was also the mechanism of crack self-healing. However, the characteristic peak of $CaCO_3$ appeared in the XRD pattern for the AS-28 days sample, which was due to the sample's long-term contact with CO_2 in the air during the curing process

TABLE 3 Measuring parameter.

Test project	Major parameter
Portal infiltration analysis	HKY/DRD-1 gas permeability automatic tester, sample size is *f* 25 mm*50 mm, measuring range is 0.01–10,000*10^{-3} md; test temperature is room temperature, and test working medium is nitrogen. Ultrapore-300 automatic helium porosity meter to determine the sample porosity, the tested environment was helium, with a pressure of 1.379 MPa, a room temperature, and a measurement range of 0.01%–40%
μ-CT	Samples were scanned with an X-ray energy at 240 kV and 312 W
ESEM&EDX	The operating voltage in the test environment is 20 V-30 KV, and the magnification of the equipment is 100–10,000 X
XRD	Phase analysis was scanned from the range of 5–70 at a rate of 0.04/s

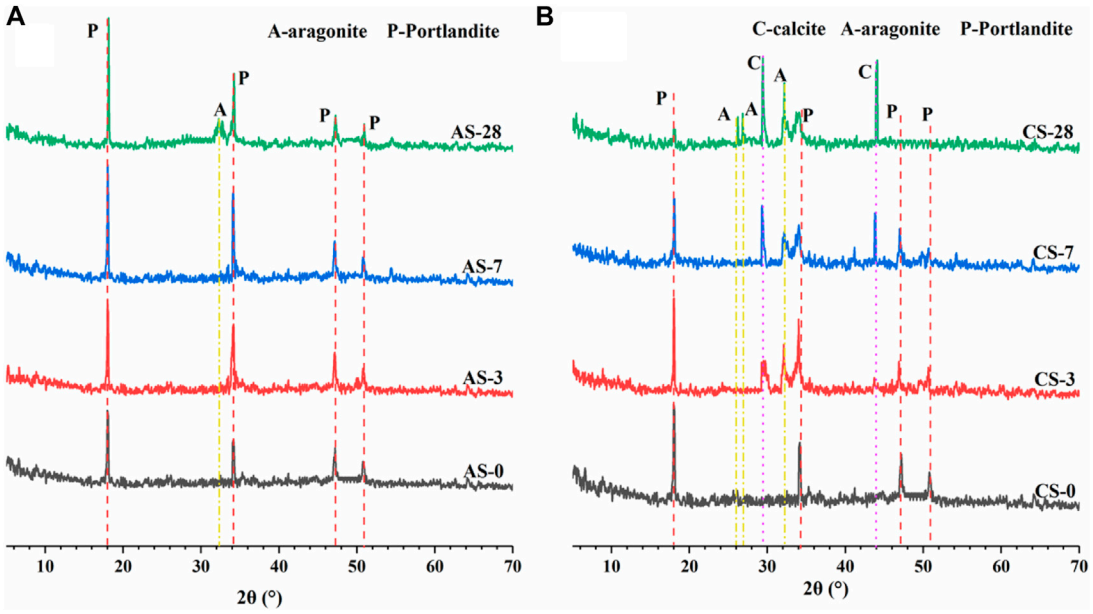

FIGURE 2
XRD analysis results for the self-healing product in the surface cracks of the **(A)** control and **(B)** self-healing samples.

(Gu et al., 2017; Mei et al., 2018). Figure 2B presents the XRD patterns of the CS samples. The characteristic peaks of CH were observed at 2θ = 18.0°,34.1°, 47.1°, and 50.8°. As the self-healing process continued, the CH peak strength of the sample began decreased, and characteristic peaks of aragonite (PDF# 00-003-1067) and calcite (PDF # 01-083-0577) appeared. In the late stage of healing, the peak strength of aragonite decreased, and the peak strength of calcite gradually increased. This was due to the conversion of some aragonite to calcite. It was previously reported that the three most common forms of $CaCO_3$ crystals are calcite, vaterite (PDF # 01-074-1867), and aragonite (PDF# 00-003-1067) (Bertier et al., 2006). Calcite crystals are relatively intact and have good stability, while vaterite has poor crystallinity and low stability (He and hui Yang, 2012). The stability of aragonite is between those of calcite and vaterite, and crystal polymorphism usually occurs at high pressures (Reeder, 1984). Studies have suggested that calcite is formed by the carbonation of CH and that the carbonation of C-S-H gel produces vaterite and aragonite with a low stability and poor crystallinity (Villain et al., 2007). The results indicate that CO_2 causes the hydration products of cement particles to form $CaCO_3$ and be deposited on the crack surface. This is the main mechanism of CS sample self-healing, which differs from the self-healing mechanism of AS samples. With an increase in the cracking age, the intensity of the CH characteristic peaks for the CS samples first increased and then decreased, and the intensity of the $CaCO_3$ characteristic peaks gradually increased. Overall, the XRD results indicated that the main self-healing products in the CS and AS samples were $CaCO_3$ and CH, respectively. The XRD patterns of the CS samples

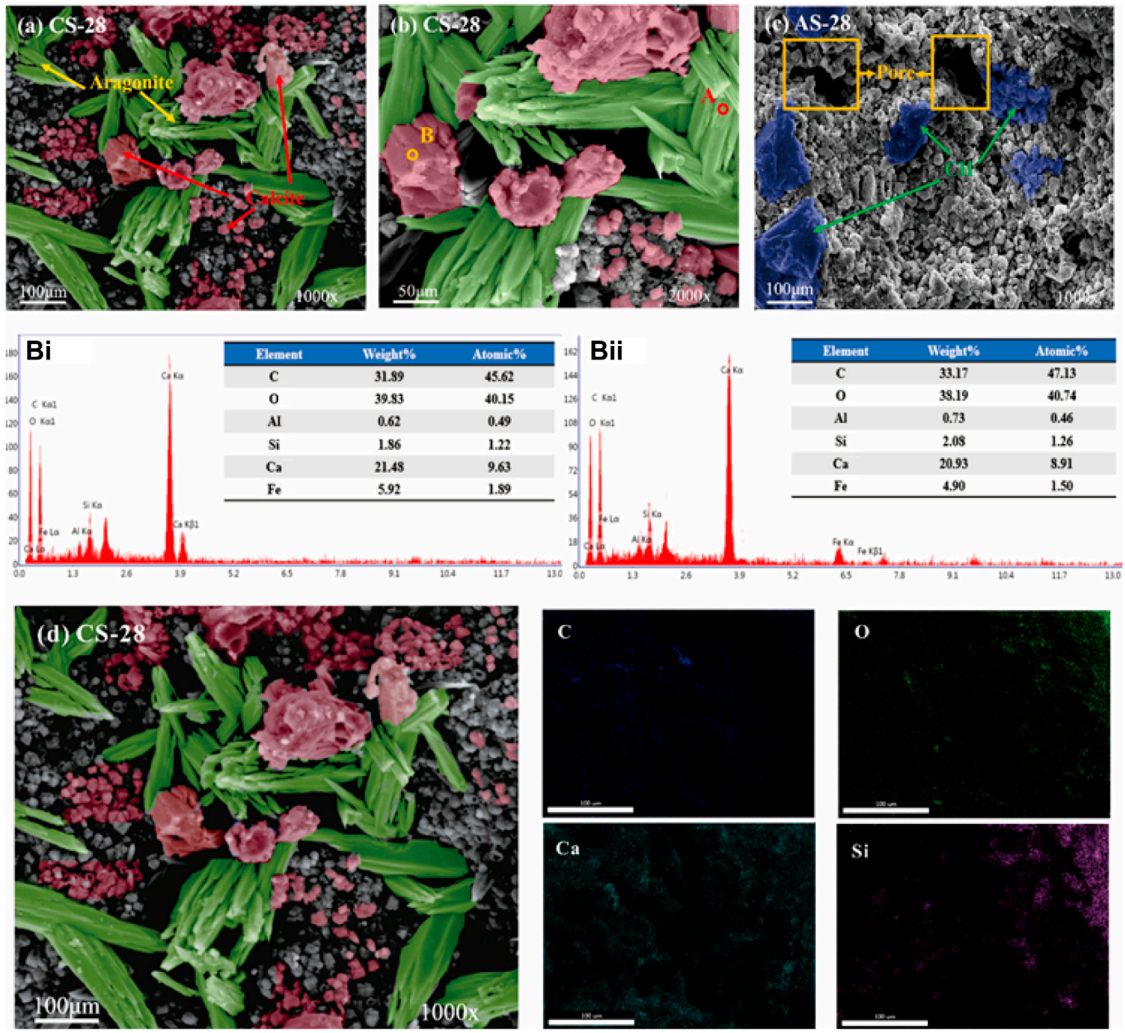

FIGURE 3
ESEM photographs of the self-healing products on the crack surface of the sample and crack surface: **(A)** CS-28 sample; **(B)** CS-28 sample material magnified 2000 times; **(C)** AS-28 sample; **(Bi)** EDX spectrum of point A in **(B)**; **(Bii)** EDX spectrum of point B in **(B)**; **(D)** elemental maps **(C,O, Ca,** and **Si)** of the cracked surface of the CS-28 specimen.

indicated that the crystal transformation of CH to $CaCO_3$ mostly resulted in calcite and aragonite, in agreement with previous research on self-healing products (Tang et al., 2015).

ESEM and EDX analysis

To further investigate the self-healing mechanism of the CO_2-induced $CaCO_3$ deposition, the elements and micromorphology of the self-healing products were analyzed using ESEM-EDX technology. Figure 3 shows ESEM images of CS-28 and AS-28 specimens and the EDX spectra of the healing products. As shown in Figure 3A, there were numerous massive (calcite) and needle-like (aragonite) materials on the crack surface of the CS-28 sample. Observation at a magnification of ×2000 revealed healing products of different sizes, as shown in Figure 3B. The EDX results (Figures 3Bi,Bii) indicated that the main elements of these substances were C, O, and Ca, and the wide and uniform distribution of these elements (as shown in Figure 3D) confirmed the formation of self-healing products ($CaCO_3$). As shown in Figure 3C, no $CaCO_3$ crystals appeared on the cracked surface of the AS-28 sample.

These results indicate that the self-healing mechanism of CO_2 induced $CaCO_3$ deposition, as shown in Figure 4. When the crack self-heals, the water in the crack can quickly migrate to the interior of the matrix. As the most soluble hydration product in the matrix, CH easily leaches from the matrix and migrates into the pores or cracks (Gwon et al., 2019). Simultaneously, Ca^{2+}

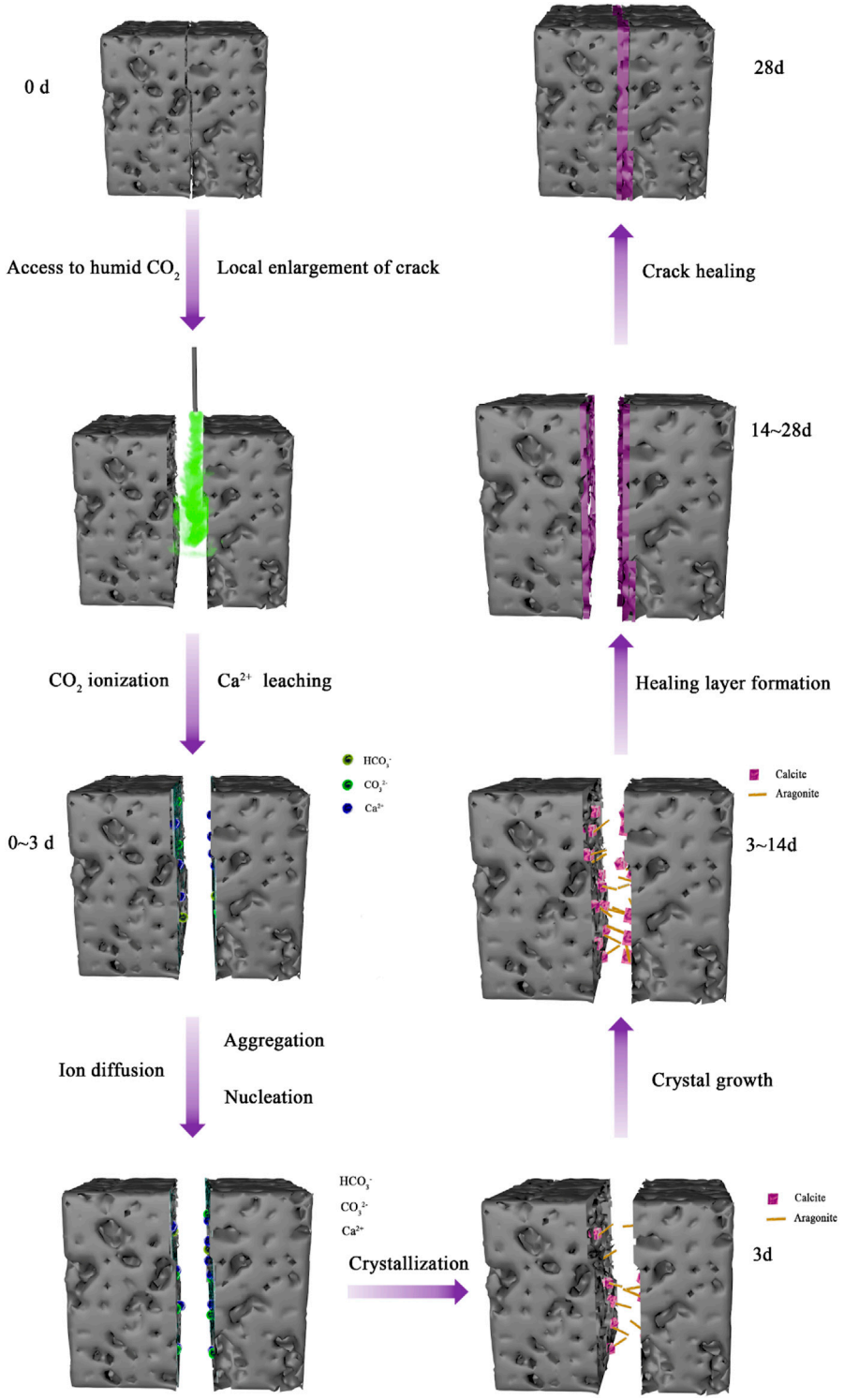

FIGURE 4
Self-healing mechanism of CO_2-induced $CaCO_3$ deposition.

reacts with CO_3^{2-} formed by CO_2 dissolved in water, generating $CaCO_3$ microcrystals, in agreement with the XRD and EDX analysis results for the self-healing reaction products. Additionally, this is consistent with the previous research results (Qian et al., 2009; Sisomphon et al., 2012). In a water-wet environment, $CaCO_3$ microcrystals have a nucleation effect,

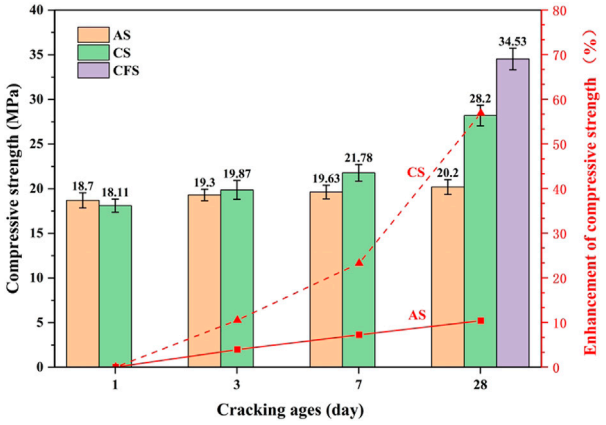

FIGURE 5
Compressive-strength results for the self-healing and control samples (CFS: cracks free sample after 28 days of curing).

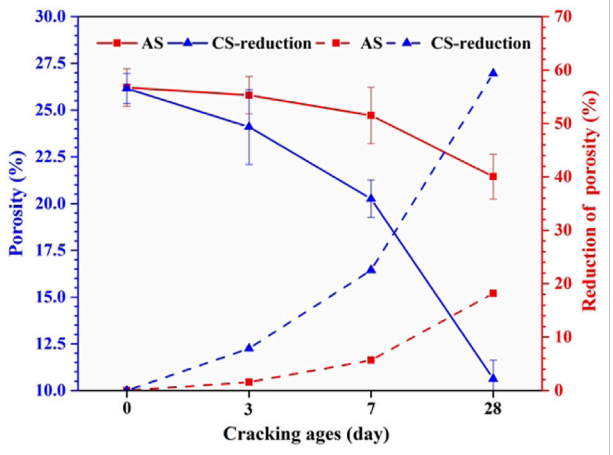

FIGURE 6
Results of the porosity test after self-healing of cement-based materials.

which is beneficial to Ca^{2+} migration out of the matrix and accelerates the $CaCO_3$ deposition. Over time, $CaCO_3$ crystals develop and grow, forming $CaCO_3$ particles of different morphologies and sizes, which help to divide the crack gaps and blocked pore channels. These $CaCO_3$ crystals (as a self-healing product) can promote crack healing, improving the microstructure of cement-based materials and restoring their mechanical properties.

Compressive strength

The results for the compressive strength of the CS and AS samples after different period after cracking are presented in Figure 5. CFS means the sample before the crack is made. As shown, with an increase in the cracking period, the compressive strengths of the CS and AS samples increased to varying degrees. The compressive strengths of the CS-28 and AS-28 samples increased to 28.20 ± 1.15 and 20.20 ± 0.83 MPa, respectively. Compared with the compressive strengths of the samples at 0 days of cracking, the compressive strengths of the CS-28 and AS-28 samples were increased by 56.67% and 10.38%, respectively. The compressive strength of CS-28 is lower than that of CFS. This is because the cracks on the edge of the CS-28 have not fully healed.

According to the compressive-strength results, all the samples underwent the process of self-healing, but owing to the different environments of the samples, the increases in the compressive strength varied significantly. As indicated by previous studies (Tang et al., 2015), the autogenous self-healing process is mainly dependent on one or more of the following four mechanisms: 1) The deposition of $CaCO_3$ formed by Calcium leaching (Kutchko et al., 2007; Brunet et al., 2013)]; 2) debris deposition in a water environment (Barlet-Gouédard et al., 2007); 3) unhydrated cement particles; and the 4) expansion of hydration products (Walsh et al., 2013). In this study, because the CS and AS samples were in different environments, the self-healing mechanisms of the two samples were different. The self-healing process of the CS samples depended on the $CaCO_3$ deposits formed by CH and the hydration of the unhydrated cement particles, while that of the AS samples depended on the hydration of the unhydrated particles. Comparing the compressive-strength results for the CS and AS samples revealed that the self-healing effect of the CS samples was better than that of the AS samples. The compressive-strength results indicated that hydration of unhydrated cement particles in the sample did not achieve the self-healing effect and that CO_2 was beneficial to the formation of $CaCO_3$ in the cement matrix, promoting the self-healing and restoring the mechanical properties of the sample.

Porosity and permeability

The test results for the porosity of the sample obtained using the gas method are presented in Figure 6. The porosity trends of the CS and AS samples were consistent; in both cases, the porosity decreased with an increase in the cracking age. However, compared with the AS sample, the porosity of the CS sample decreased more significantly, with a larger amplitude and faster rate. After the cracking age reached 28 days, the porosity of the CS-28 sample was 10.63%, while the porosity of the AS-28 sample was 21.44% (2.02 times that of the CS-28 sample). The porosity recovery rates of the CS-28 and AS-28 samples were 59.37% and 18.19%, respectively. The porosity of CS-28 is significantly higher than that of CFS. In addition to the

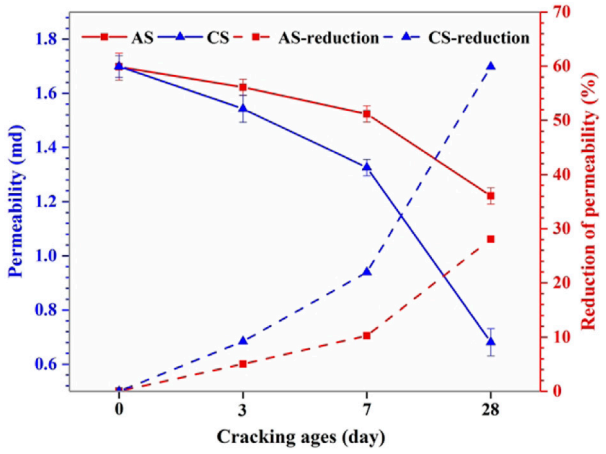

FIGURE 7
Results of the permeability test after self-healing of cement-based material.

incomplete healing of the cracks on the edge of CS-28, the dissolution of calcium hydroxide in the pores and the leaching of calcium from the silica gel layer will increase the porosity of the cement matrix. Therefore, CFS has a lower permeability than CS-28.

The permeability of the samples after self-healing was tested using an air permeability automatic tester, and the results are shown in Figure 7. The permeability of the CS and AS samples decreased with an increase in the cracking age. After the cracking age reached 28 days, the permeability values of the CS-28 and AS-28 samples were 0.6812 and 1.2213 md (1.79 times that of the CS-28 sample), respectively. According to the experimental results, the permeability recovery degrees of the samples were calculated (59.91% and 28.07% for the CS-28 and AS-28 samples, respectively). The permeability of CFS is less than 200 μD, which shows that cement without cracks can prevent CO_2 leakage. With the healing of the cracks in the edge of CS-28, the permeability of CS-28 will be further reduced.

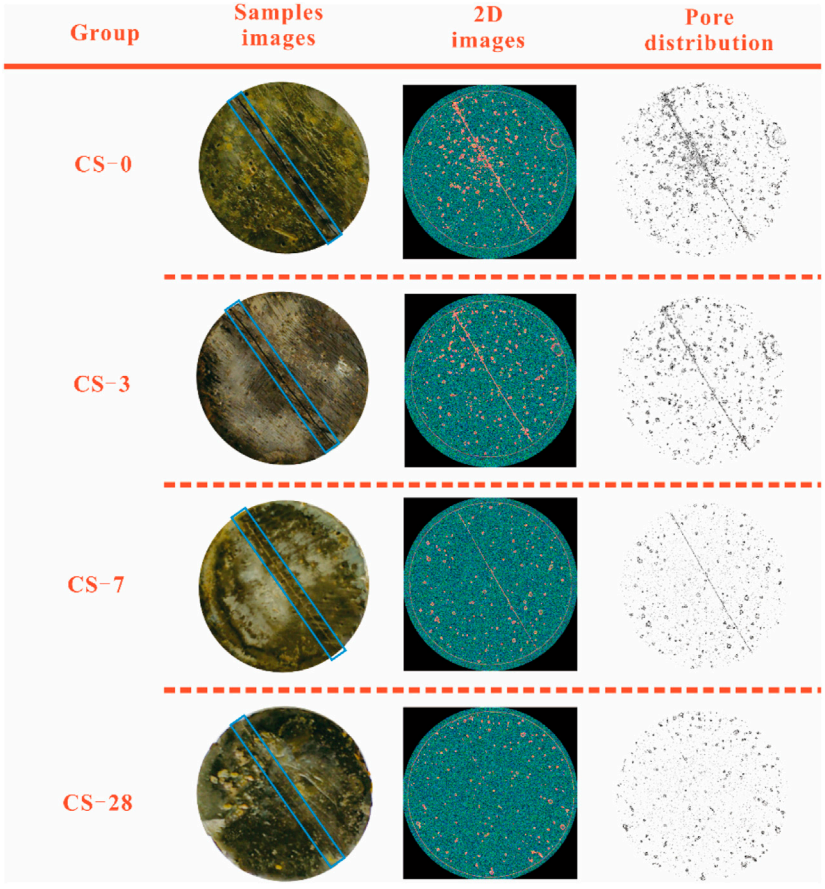

FIGURE 8
2D vertical section taken from the *Z*-axis of the CS sample.

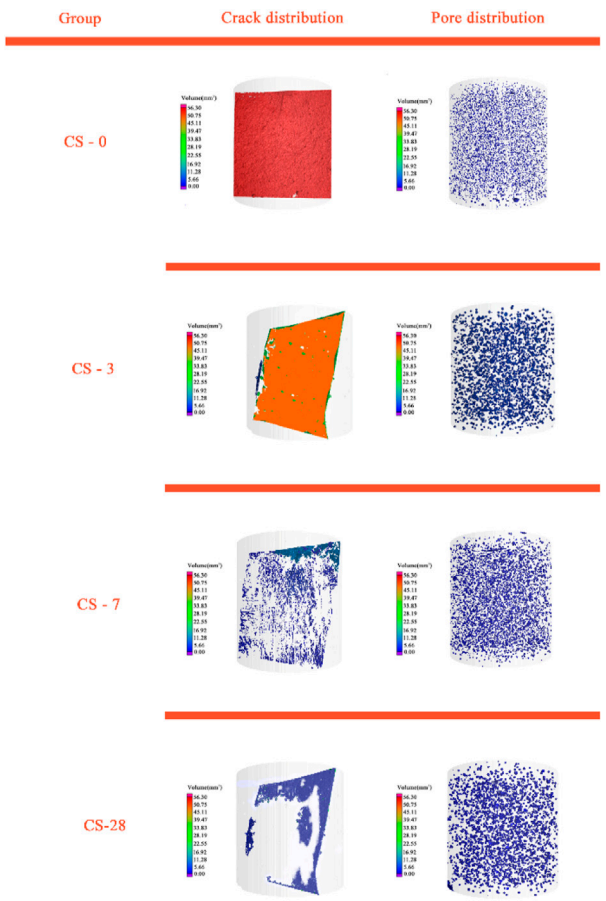

FIGURE 9
X-ray μCT scan 3D images of self-healing samples.

In general, the porosity and permeability results indicate that in the CS samples, a large amount of $CaCO_3$ was deposited on the cracks, which significantly accelerated the self-healing of the cracks. Additionally, the small $CaCO_3$ particles filled the pores of the CS sample, significantly reducing its porosity and permeability. In the AS sample, owing to the presence of a certain amount of unhydrated cement particles, minerals, and primary hydration products, the pores were filled to a certain extent through further hydration, reducing the porosity and permeability of the sample. This trend was weakened with an increase in the cracking ages, and the filling effect was far from satisfying the self-healing requirements. The self-healing ability and degree of the CS samples were significantly greater than those of the AS samples. These results indicate that autogenous self-healing of a cement-based material primarily depends on the surrounding environment (Bertier et al., 2006; Wang et al., 2014b; Luo et al., 2015) and that CO_2 can induce the formation of calcium carbonate in cement-based materials, accelerating the self-healing process. The porosity and permeability results are consistent with the self-healing ability and strength recovery performance of cracks.

X-ray computed tomography

X-ray computed tomography is an imaging technique in which digital geometric processing is used to generate three-dimensional (3D) images of scanned samples. To observe the crack volume change due to self-healing, the software VGStudio MAX 2.0 was used to visualize and analyze the 3D data. The software can import data of different types, sizes, and proportions to measure objects in multiple areas.

Figure 8 shows 2D images of typical crack contours and pore structures of self-healing specimens at different cracking ages. From the vertical physical map and 2D images, the typical image of the cracks in the CS-7 specimens after healing can be seen, and the pre-existing cracks can hardly be seen. These cracks were covered by some white matter, and after testing and analyzing the white matter, it was found to be calcium carbonate. As the cracking age increased, the cracks are gradually filled with healing products and form a healing layer. The amount of pores in the matrix gradually decreased, and the self-healing efficiency increased. However, it is difficult to obtain a general overview of the 3D distribution of sample pores and crack healing from 2D slices, so that they can be quantitatively compared. Therefore, 2D reconstructed slices are presented as 3D to obtain a complete 3D view of the distribution of pore in the entire sample.

Figure 9 shows 3D images of cracks and pore structures of self-healing specimens at different cracking ages. Although the number of cracks and pores is gradually reduced in the 2D image, it does not indicate the changes in the distribution of cracks and pores inside and deep in the sample, and the 3D image can solve

TABLE 4 Changes in the crack volume and pore volume of the CS samples.

Sample	Crack volume (mm^3)	Crack-volume reduction rate (%)	Pore volume (mm^3)	Pore-volume reduction rate (%)
CS-0	46.38	0	88.03	0
CS-3	43.65	5.89	84.93	3.52
CS-7	34.86	24.84	72.65	17.47
CS-28	15.27	57.08	27.11	69.20

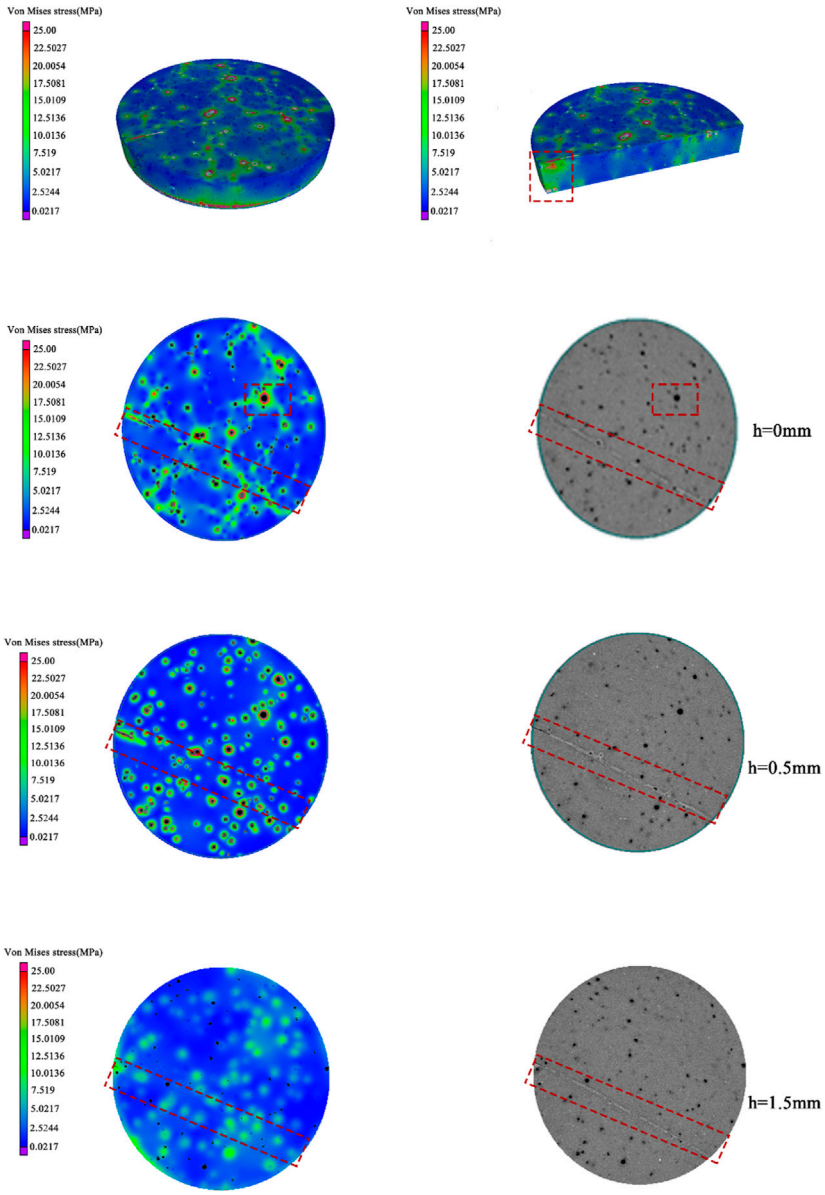

FIGURE 10
Von mises stress distribution of the healed cement matrix.

this problem well. It can be seen from the image of the change in the 3D distribution of the cement sample that with the progress of the self-healing process, the volume of pore and crack show a downward trend. This indicates that the deposition of self-healing products inside the sample is not only distributed around the crack, but randomly distributed throughout the sample. However, Ca^{2+} involved in the formation of calcium carbonate is provided by calcium hydroxide (Kutchko et al., 2007) in the pores and C-S-H (Brunet et al., 2013) of the cement matrix. In a humid environment, Ca^{2+} dissolves and nucleates on the crack surface to form $CaCO_3$. The presence of cracks provides a channel for moist CO_2 gas, allowing large amounts of calcium carbonate to be deposited at the cracks, accelerating the healing of the cracks. This is also the reason why denser calcium carbonate deposits are found at the cracks.

The changes in the crack volume and pore volume are presented in Table 4. The CS-28 specimen had a crack volume of 15.27 mm^3 and a pore volume of 27.11 mm^3. The crack-volume reduction rate was 57.08%, and the pore-volume reduction rate was 69.20%. The rapid self-healing reaction is based on the convective flow of supercritical CO_2 on the crack surface (Domenico et al., 1998). However, for cement

matrix, the carbonation reaction in the pores depends on the penetration and diffusion of supercritical CO_2 (Huet et al., 2006). Generally, the permeability of cement matrix is less than 200 μD (Kutchko et al., 2009), which limits the carbonization reaction in the pores of cement matrix. In this case, the dissolution of calcium hydroxide in the pores and the calcium leaching of the silica gel layer lead to the increasing of porosity of the cement matrix (Urbonas et al., 2016). This is the reason about CS-0 has much less pores than CS-28. In addition, due to the factor of splitting the experimental mold, the width of the crack on the outer edges is larger than the middle of the sample. This is the reason about the crack face disappears in the middle of the sample but is still visible at the outer edges for CS-28.

Additionally, the images from the X-ray μCT scan indicated that the products produced by the self-healing effect were mainly concentrated on the crack surface and in the matrix pores. This is because the Ca^{2+} in the matrix leached out and migrated to the crack surface, reacted with CO_3^{2-} and HCO_3^- to form $CaCO_3$ of different sizes, and filled pores and cracks (Sisomphon et al., 2012). Therefore, as the cracking age increased, the amounts of cracks and pores decreased significantly. Wang et al. (Wang et al., 2014a) reported similar findings when they studied the self-healing properties of concrete specimens incorporated with hydrogel-encapsulated bacterial spores; the self-healing effect was mainly limited to cracked surfaces. Generally, in a high-concentration CO_2 environment, CO_2 accelerates the deposition of calcium carbonate, promotes the self-healing of cracks, and can effectively recover various properties of cement-based materials.

Von mises stress distribution simulation

The Von-Mises stress is an equivalent stress, which can reflect the yield state of the cement-based materials, and also can represent the stress and strain states comprehensively of the cement-based materials (Mendez Restrepo et al., 2020). Forces were simulated along the axial direction of the CS-28, and the stress distribution of the healed cement matrix was analysed using VGStudio MAX 3.0 software. In order to simplify the calculation process and improve the calculation accuracy, a sample with a height of 3 mm was selected in the middle of the healed cement matrix for calculation. The simulation results are shown in Figure 10. Observing the cut surface of the healing layer, it can be found that under the axial force, the von Mises stress only has a stress concentration point on the edge of the force surface. The von Mises stress distribution of cross-sections of different heights shows that the closer to the stress surface, the easier it is for the healed cement matrix to form stress concentration points. The unhealed gap between the healing layer and the cement matrix is the main reason for the existence of von Mises stress concentration points in the healed layer. In addition, the von Mises stress formed at the large pores of the cement matrix is larger than the von Mises stress at the healing layer, which indicates that the pores of the cement matrix are more likely to be damaged than the pores of the healing layer under axial force.

Conclusion and prospect

The self-healing mechanism and products of cracks in cement-based materials in a CO_2-rich environment were investigated. The changes in the crack-filling rate were analyzed with respect to the cracking age, and the self-healing reaction products of the cracks were characterized. According to the experimental results, the following conclusions are drawn.

(1) The compressive strength of the cement-based materials increased with the cracking age. The compressive strengths of the CS-28 and AS-28 samples were 28.20 ± 1.15 and 20.20 ± 0.83 MPa, respectively. The compressive-strength recovery rates were 56.67% and 10.38%.
(2) The porosity and permeability of the cement-based materials exhibited similar trends; both decreased with an increase in the cracking age. The porosity values of the CS-28 and AS-28 samples were 10.63% and 21.44%, and the recovery rates of the porosity were 59.37% and 18.19%, respectively. The permeability values of the CS-28 and AS-28 samples were 0.6812 and 1.2213 md, respectively, and the permeability recovery rates were 59.91% and 28.07%, respectively, the porosity and permeability results indicate that the self-healing ability and extent were significantly greater for the CS samples than for the AS samples.
(3) X-ray μ-CT indicated that the products produced by the self-healing effect were mainly concentrated in the crack surface and matrix pores. The CS-28 specimen had a crack volume of 15.27 mm^3 and a pore volume of 27.11 mm^3. The crack-volume reduction rate was 57.08%, and the pore-volume reduction rate was 69.20%.
(4) ESEM indicated that massive, needle-shaped self-healing products existed at the crack-healing site. XRD and EDX analysis revealed that the surface substance was calcite and aragonite.
(5) The von Mises stress distribution of the healed cement matrix was simulated by the finite element method and the damage prediction was performed. Under the axial force, the healing layer formed is less prone to damage than the pores of the cement matrix.

Although this study evaluates the self-healing situation of cement-based materials in the downhole environment based on

temperature, medium state and age, but the self-healing situation under the combined action of various influencing factors needs further research. In addition, the selection and self-healing evaluation of exogenous calcium carbonate crystallization-inducing substances is not performed herein. In the subsequent research, the self-healing ability and influencing factors of the hybrid fiber or whisker material on the cement-based material in the complex underground environment can be carried out.

Data availability statement

The original contributions presented in the study are included in the article/supplementary material, further inquiries can be directed to the corresponding author.

Author contributions

XX: Conceptualization, investigation, writing-original draft, data curation GZ: Validation, resources, writing—review and editing, supervision. ZW: Validation, formal analysis, investigation, data curation JC: Formal analysis, project administration XC: Methodology, conceptualization.

Acknowledgments

The authors appreciate the support of the Sichuan Science and Technology Program (2021YFQ0045 and 2021YFSY0056) and the Cnooc's preliminary project: Feasibility study of Wenchang 9-7 oilfield (2021PFS-05). The authors would also like to thank the Advanced Cementing Materials Research Center of SWPU for their kind assistance with the experiments.

Conflict of interest

The authors declare that the research was conducted in the absence of any commercial or financial relationships that could be construed as a potential conflict of interest.

Publisher's note

References

Abid, K., Gholami, R., and Mutadir, G. (2020). A pozzolanic based methodology to reinforce Portland cement used for CO_2 storage sites. *J. Nat. Gas. Sci. Eng.* 73, 103062. doi:10.1016/j.jngse.2019.103062

API-RP-10B-2 (2013). "Recommended practice for testing well cements," in *200 Massachusetts avenue NW suite 1100* (Washington, DC United States: American Petroleum Institute).

Bachu, S., and Watson, T. L. (2009). Review of failures for wells used for CO_2 and acid gas injection in Alberta, Canada. *Energy Procedia* 1, 3531–3537. doi:10.1016/j.egypro.2009.02.146

Barlet-Gouédard, V., Rimmelé, G., Goffé, B., and Porcherie, O. (2007). Well technologies for CO_2 geological storage: CO_2-Resistant cement. *Oil Gas Sci. Technol. - Rev. IFP.* 62, 325–334. doi:10.2516/ogst:2007027

Bertier, P., Swennen, R., Laenen, B., Lagrou, D., and Dreesen, R. (2006). Experimental identification of CO_2-water-rock interactions caused by sequestration of CO_2 in Westphalian and Buntsandstein sandstones of the Campine Basin (NE-Belgium). *J. Geochem. Explor.* 89, 10–14. doi:10.1016/j.gexplo.2005.11.005

Brunet, J. P. L., Li, L., Karpyn, Z. T., Kutchko, B. G., Strazisar, B., and Bromhal, G. (2013). Dynamic evolution of cement composition and transport properties under conditions relevant to geological carbon sequestration. *Energy fuels.* 27, 4208–4220. doi:10.1021/ef302023v

Costa, B. L. S., Freitas, J. C. de O., Santos, P. H. S., Melo, D. M. de A., and de Oliveira, Y. H. (2017). Effects of carbon dioxide in Portland cement: A relation between static sedimentation and carbonation. *Constr. Build. Mat.* 150, 450–458. doi:10.1016/j.conbuildmat.2017.06.021

Costa, I., Rochedo, P., Costa, D., Ferreira, P., Araújo, M., Schaeffer, R., et al. (2019). Placing hubs in CO_2 pipelines : An application to industrial CO_2 emissions in the Iberian Peninsula. *Appl. Energy* 236, 22–31. doi:10.1016/j.apenergy.2018.11.050

Dindi, A., Quang, D. V., Vega, L. F., Nashef, E., and Abu-Zahra, M. R. (2019). Applications of fly ash for CO_2 capture, utilization, and storage. *J. CO_2 Util.* 29, 82–102. doi:10.1016/j.jcou.2018.11.011

Domenico, P. A., Harris, D. B., Schwartz, F. W., and Wiley, J. (1998). *Physical and chemical hydrogeology*. Wiley, 215.

Duguid, A., and Scherer, G. W. (2010). Degradation of oilwell cement due to exposure to carbonated brine. *Int. J. Greenh. Gas Control* 4, 546–560. doi:10.1016/j.ijggc.2009.11.001

Energy Institute (2010). *Good plant design and operation for onshore carbon capture installations and onshore pipelines*. Energy Institute and the Global Carbon Capture and Storage Institute, 137.

Ferrara, L., Krelani, V., Moretti, F., Roig, M., and Serna, P. (2017). Effects of autogenous healing on the recovery of mechanical performance of high performance fibre reinforced cementitious composites (HPFRCCs): Part 1. *Cem. Concr. Compos.* 83, 76–100. doi:10.1016/j.cemconcomp.2017.07.010

Garcia, M., Berghout, N., Energy, I., Gas, A.-G., Ieaghg, P., Offices, P., et al. (2019). Toward a common method of cost-review for carbon capture technologies in the industrial sector : Cement and iron and steel plants. *Int. J. Greenh. Gas Control* 87, 142–158. doi:10.1016/j.ijggc.2019.05.005

Gerres, T., Avila, P. C., Llamas, P. L., and San Roman, T. G. (2019). A review of cross-sector decarbonisation potentials in the European energy intensive industry. *J. Clean. Prod.* 210, 585–601. doi:10.1016/j.jclepro.2018.11.036

Gu, T., Guo, X., Li, Z., Cheng, X., Fan, X., Korayem, A., et al. (2017). Coupled effect of CO_2 attack and tensile stress on well cement under CO_2 storage conditions. *Constr. Build. Mat.* 130, 92–102. doi:10.1016/j.conbuildmat.2016.10.117

Gupta, S., Wei, H., and Dai, S. (2018). Healing cement mortar by immobilization of bacteria in biochar: An integrated approach of self-healing and carbon sequestration. *Cem. Concr. Compos.* 86, 238–254. doi:10.1016/j.cemconcomp.2017.11.015

Gwon, S., Ahn, E., and Shin, M. (2019). Self-healing of modified sulfur composites with calcium sulfoaluminate cement and superabsorbent polymer. *Compos. Part B Eng.* 162, 469–483. doi:10.1016/j.compositesb.2019.01.003

He, J., and hui Yang, C. (2012). Influence of carbonation on microstructure of alkali-activated slag cement pastes. *J. Build. Mat.* 15, 1–5. doi:10.3969/j.issn.1007-9629.2012.01.024

Huang, H., Ye, G., and Damidot, D. (2013). Characterization and quantification of self-healing behaviors of microcracks due to further hydration in cement paste. *Cem. Concr. Res.* 52, 71–81. doi:10.1016/j.cemconres.2013.05.003

Huet, B., Fuller, R., and Prevost, J. (2006). Development of a coupled geochemical transport code to simulate cement degradation in CO_2 saturated brine. *Eighth Int. Conf. Greenh. Gas. Control Technol.*

Jiang, Z., Li, W., and Yuan, Z. (2015). Influence of mineral additives and environmental conditions on the self-healing capabilities of cementitious materials. *Cem. Concr. Compos.* 57, 116–127. doi:10.1016/j.cemconcomp.2014.11.014

Jung, H. B., and Um, W. (2013). Experimental study of potential wellbore cement carbonation by various phases of carbon dioxide during geologic carbon sequestration. *Appl. Geochem.* 35, 161–172. doi:10.1016/j.apgeochem.2013.04.007

Klemm, A. J., and Sikora, K. S. (2013). The effect of Superabsorbent Polymers (SAP) on microstructure and mechanical properties of fly ash cementitious mortars. *Constr. Build. Mat.* 49, 134–143. doi:10.1016/j.conbuildmat.2013.07.039

Kutchko, B. G., Strazisar, B. R., Dzombak, D. A., Lowry, G. V., and Thaulow, N. (2007). Degradation of well cement by CO_2 under geologic sequestration conditions. *Environ. Sci. Technol.* 41, 4787–4792. doi:10.1021/es062828c

Kutchko, B. G., Strazisar, B. R., Huerta, N., Lowry, G. V., Dzombak, D. A., and Thaulow, N. (2009). CO_2 reaction with hydrated class H well cement under geologic sequestration conditions: Effects of flyash admixtures. *Environ. Sci. Technol.* 43, 3947–3952. doi:10.1021/es803007e

Leung, D. Y. C., Caramanna, G., and Maroto-valer, M. M. (2014). An overview of current status of carbon dioxide capture and storage technologies. *Renew. Sustain. Energy Rev.* 39, 426–443. doi:10.1016/j.rser.2014.07.093

Li, Q., Liu, Z., Chen, W., Yuan, B., Liu, X., and Chen, W. (2019). A novel bio-inspired bone-mimic self-healing cement paste based on hydroxyapatite formation. *Cem. Concr. Compos.* 104, 103357. doi:10.1016/j.cemconcomp.2019.103357

Liu, J., Ou, Z., Mo, J., Wang, Y., and Wu, H. (2017). The effect of SCMs and SAP on the autogenous shrinkage and hydration process of RPC. *Constr. Build. Mat.* 155, 239–249. doi:10.1016/j.conbuildmat.2017.08.061

Luo, M., Qian, C. X., and Li, R. Y. (2015). Factors affecting crack repairing capacity of bacteria-based self-healing concrete. *Constr. Build. Mat.* 87, 1–7. doi:10.1016/j.conbuildmat.2015.03.117

Mei, K., Cheng, X., Zhang, H., Yu, Y., Gao, X., Zhao, F., et al. (2018). The coupled reaction and crystal growth mechanism of tricalcium silicate (C_3S): An experimental study for carbon dioxide geo-sequestration wells. *Constr. Build. Mat.* 187, 1286–1294. doi:10.1016/j.conbuildmat.2018.08.080

Mendez Restrepo, M., Teodoriu, C., Salehi, S., and Wu, X. (2020). A novel way to look at the cement sheath integrity by introducing the existence of empty spaces inside of the cement (voids). *J. Nat. Gas Sci. Eng.* 77, 103274. doi:10.1016/j.jngse.2020.103274

Nakicenovic, Z., Alcamo, J., Davis, G., Vries, B. D., Fenhann, J. V., and Gaffin, S. (2000). "Special report on emissions scenarios," in *Special report of working group III of the intergovernmental panel on climate change* (Cambridge University Press).

Palin, D., Wiktor, V., and Jonkers, H. M. (2015). Autogenous healing of marine exposed concrete : Characterization and quanti fi cation through visual crack closure. *Cem. Concr. Res.* 73, 17–24. doi:10.1016/j.cemconres.2015.02.021

Pejman, A., Rishi, G., and Alireza, B. (2019). Assessment of self-healing and durability parameters of concretes incorporating crystalline admixtures and Portland Limestone Cement. *Cem. Concr. Compos.* 99, 17–31. doi:10.1016/j.cemconcomp.2019.02.017

Qian, S., Zhou, J., de Rooij, M. R., Schlangen, E., Ye, G., and van Breugel, K. (2009). Self-healing behavior of strain hardening cementitious composites incorporating local waste materials. *Cem. Concr. Compos.* 31, 613–621. doi:10.1016/j.cemconcomp.2009.03.003

Reeder, R. J. (1984). Carbonates:Mineralogy and chemistry. *Geochim. Cosmochim. Acta* 48, 1387–1388. doi:10.1016/0016-7037(84)90083-8

Roig-Flores, M., Moscato, S., Serna, P., and Ferrara, L. (2015). Self-healing capability of concrete with crystalline admixtures in different environments. *Constr. Build. Mat.* 86, 1–11. doi:10.1016/j.conbuildmat.2015.03.091

Rupnow, T., Asce, M., and Mohammad, L. N. (2017). Characterization of self-healing processes induced by calcium nitrate microcapsules in cement mortar. *J. Mat. Civ. Eng.* 29, 1–10. doi:10.1061/(ASCE)MT.1943-5533.0001717

Sahmaran, M., Yildirim, G., and Erdem, T. K. (2013). Self-healing capability of cementitious composites incorporating different supplementary cementitious materials. *Cem. Concr. Compos.* 35 (1), 89–101. doi:10.1016/j.cemconcomp.2012.08.013

Shah, V., and Bishnoi, S. (2018). Carbonation resistance of cements containing supplementary cementitious materials and its relation to various parameters of concrete. *Constr. Build. Mat.* 178, 219–232. doi:10.1016/j.conbuildmat.2018.05.162

Sisomphon, K., Copuroglu, O., and Koenders, E. A. B. (2012). Self-healing of surface cracks in mortars with expansive additive and crystalline additive. *Cem. Concr. Compos.* 34, 566–574. doi:10.1016/j.cemconcomp.2012.01.005

Su, Y., Feng, J., Jin, P., and Qian, C. (2019). Influence of bacterial self-healing agent on early age performance of cement-based materials. *Constr. Build. Mat.* 218, 224–234. doi:10.1016/j.conbuildmat.2019.05.077

Suleiman, A. R., and Nehdi, M. L. (2018). Effect of environmental exposure on autogenous self-healing of cracked cement-based materials. *Cem. Concr. Res.* 111, 197–208. doi:10.1016/j.cemconres.2018.05.009

Suleiman, A. R., Nelson, A. J., and Nehdi, M. L. (2019). Visualization and quantification of crack self-healing in cement-based materials incorporating different minerals. *Cem. Concr. Compos.* 103, 49–58. doi:10.1016/j.cemconcomp.2019.04.026

Tang, W., Kardani, O., and Cui, H. (2015). Robust evaluation of self-healing efficiency in cementitious materials - a review. *Constr. Build. Mat.* 81, 233–247. doi:10.1016/j.conbuildmat.2015.02.054

Thengane, S. K., Tan, R. R., Foo, D. C. Y., and Bandyopadhyay, S. (2019). A pinch-based approach for targeting carbon capture , utilization , and storage systems. *Ind. Eng. Chem. Res.* 58, 3188–3198. doi:10.1021/acs.iecr.8b06156

Urbonas, L., Leno, V., and Heinz, D. (2016). Effect of carbonation in supercritical CO_2 on the properties of hardened cement paste of different alkalinity. *Constr. Build. Mat.* 123, 704–711. doi:10.1016/j.conbuildmat.2016.07.040

Villain, G., Thiery, M., and Platret, G. (2007). Measurement methods of carbonation profiles in concrete: Thermogravimetry, chemical analysis and gammadensimetry. *Cem. Concr. Res.* 37, 1182–1192. doi:10.1016/j.cemconres.2007.04.015

Walsh, S. D. C., Du Frane, W. L., Mason, H. E., and Carroll, S. A. (2013). Permeability of wellbore-cement fractures following degradation by carbonated brine. *Rock Mech. Rock Eng.* 46, 455–464. doi:10.1007/s00603-012-0336-9

Wang, J., Dewanckele, J., Cnudde, V., Van Vlierberghe, S., Verstraete, W., and De Belie, N. (2014). X-ray computed tomography proof of bacterial-based self-healing in concrete. *Cem. Concr. Compos.* 53, 289–304. doi:10.1016/j.cemconcomp.2014.07.014

Wang, J. Y., Soens, H., Verstraete, W., and De Belie, N. (2014). Self-healing concrete by use of microencapsulated bacterial spores. *Cem. Concr. Res.* 56, 139–152. doi:10.1016/j.cemconres.2013.11.009

Wang, R., Yu, J., Gu, S., Han, X., Peng, H., Liu, Q., et al. (2020). Effect of ion chelator on hydration process of Portland cement. *Constr. Build. Mat.* 259, 119727. doi:10.1016/j.conbuildmat.2020.119727

Wang, R., Yu, J., Gu, S., Peng, H., Du, W., Han, X., et al. (2020). Influence of ion chelator and CO_2-rich environment on self-healing capabilities of cement-based materials. *Constr. Build. Mat.* 259, 119685. doi:10.1016/j.conbuildmat.2020.119685

Wang, X. F., Fang, C., Li, D. W., Han, N., and Xing, F. (2018). A self-healing cementitious composite with mineral admixtures and built-in carbonate. *Cem. Concr. Compos.* 92, 216–229. doi:10.1016/j.cemconcomp.2018.05.013

Wang, X. F., Zhang, J. H., Zhao, W., Han, R., Han, N. X., and Xing, F. (2018). Permeability and pore structure of microcapsule-based self-healing cementitious composite. *Constr. Build. Mat.* 165, 149–162. doi:10.1016/j.conbuildmat.2017.12.008

Yuanhua, L., Dajiang, Z., Dezhi, Z., Yuanguang, Y., Taihe, S., Kuanhai, D., et al. (2013). Experimental studies on corrosion of cement in CO_2 injection wells under supercritical conditions. *Corros. Sci.* 74, 13–21. doi:10.1016/j.corsci.2013.03.018

Zha, Y., Yu, J., Wang, R., He, P., and Cao, Z. (2018). Effect of ion chelating agent on self-healing performance of Cement- based materials. *Constr. Build. Mat.* 190, 308–316. doi:10.1016/j.conbuildmat.2018.09.115

Zhang, J., Wang, J., Wang, S., Shao, S., Xiao, W., and Lin, Z. (2019). Effect of stratum on the interfacial stress and structural integrity of cement sheath. *IOP Conf. Ser. Mat. Sci. Eng.* 611, 012044. doi:10.1088/1757-899X/611/1/012044